

The upper clouds of Venus: determination of the scale height from NIMS–Galileo infrared data

M. Roos,¹ P. Drossart,¹ Th. Encrenaz,¹ E. Lellouch,¹ B. Bézard,¹ R. W. Carlson,² K. H. Baines,² L. W. Kamp,² F. W. Taylor,³ A. D. Collard,³ S. B. Calcutt,³ J. B. Pollack⁴ and D. H. Grinspoon⁵

¹ DESPA (CNRS-URA 264), Observatoire de Paris-Meudon, F-92195 Meudon, France

² Jet Propulsion Laboratory, Pasadena, CA 91109, U.S.A.

³ Clarendon Laboratory, Oxford University, Parks Road, Oxford OX1 3PU, U.K.

⁴ NASA Ames Research Center, Moffett Field, CA 94035, U.S.A.

⁵ University of Colorado, Boulder, CO 80309, U.S.A.

Abstract. The 3–5 μm thermal emission of the nightside of Venus, recorded by the NIMS instrument at the time of the *Galileo* flyby of Venus, is analysed to infer the properties of the upper cloud boundary. From the global maps of Venus at fixed wavelengths, the limb darkening of the flux is measured at several latitudes, within each infrared channel. By using the nominal *Pioneer* Venus thermal profile, these data give access to two parameters: the cloud deck temperature and the cloud scale height. It is verified independently, from the NIMS spectra, that this thermal profile is consistent with all the NIMS observations, and that the thermal structure does not vary significantly in the latitude range (25 S, 30 N). Within this range, the cloud scale height is found to be constant with latitude, and is $H = 5.2$ km, with an accuracy of about 15%, taking into account the various sources of theoretical and observational uncertainties. At higher latitudes, the temperature profile becomes more isothermal and the presented method to retrieve H is no longer valid.

Introduction

The 1990 *Galileo* flyby of Venus provided a unique opportunity to investigate the nightside of the atmosphere of Venus in the near-infrared, from the use of the NIMS (Near-Infrared Mapping Spectrometer) experiment. The first results of this exploration have been reported by Carlson *et al.* (1991). A full description of the NIMS instrument can be found in Carlson *et al.* (1992). The spectra show two well-separated regions: below 3 μm , the

radiation within selected spectral windows comes from atmospheric regions below the sulphuric acid cloud deck, where the atmospheric composition can be investigated (Kamp *et al.*, 1988); above 3 μm , due to the increasing opacity of the H_2SO_4 cloud droplets, the radiation comes from the upper cloud layer and above ($z \geq 60$ km).

As explained in Carlson *et al.* (1991), two series of data were recorded with the NIMS instrument: (1) two nightside partial global mosaics at 17 selected wavelengths (VPDIN-1 and VPDIN-2, for Venus Partial Disk Imaging Nightside), ranging from 0.7 to 5.2 μm , with a spatial resolution of about 50 km for VPDIN-1; and (2) a series of full wavelength coverage spectra of 408 spectral elements (VJBARS), taken on about 25 lines of 20 pixels each (with 1 pixel corresponding to 25 km), aligned along three meridians, about 15° of longitude apart and centred on the subspacecraft meridian.

In this paper, we analyse the long-wavelength part of the NIMS data ($\lambda \geq 3$ μm), using both the global mosaic VPDIN-1 and the full wavelength coverage spectra, in order to derive information about the upper cloud scale height and cloud temperature. A preliminary analysis of these data can be found in Carlson *et al.* (1991). First we describe the limb-darkening method; the data analysis is presented in the following for the VPDIN and VJBARS data respectively; results are presented and discussed later, and the last section summarizes our conclusions.

The limb-darkening effect

Cross-cuts have been made in the VPDIN-1 global mosaic data at different constant latitudes, in order to obtain a set of limb-darkening curves in the six discrete channels above 3.4 μm (Fig. 1), outside the strong CO_2 absorption

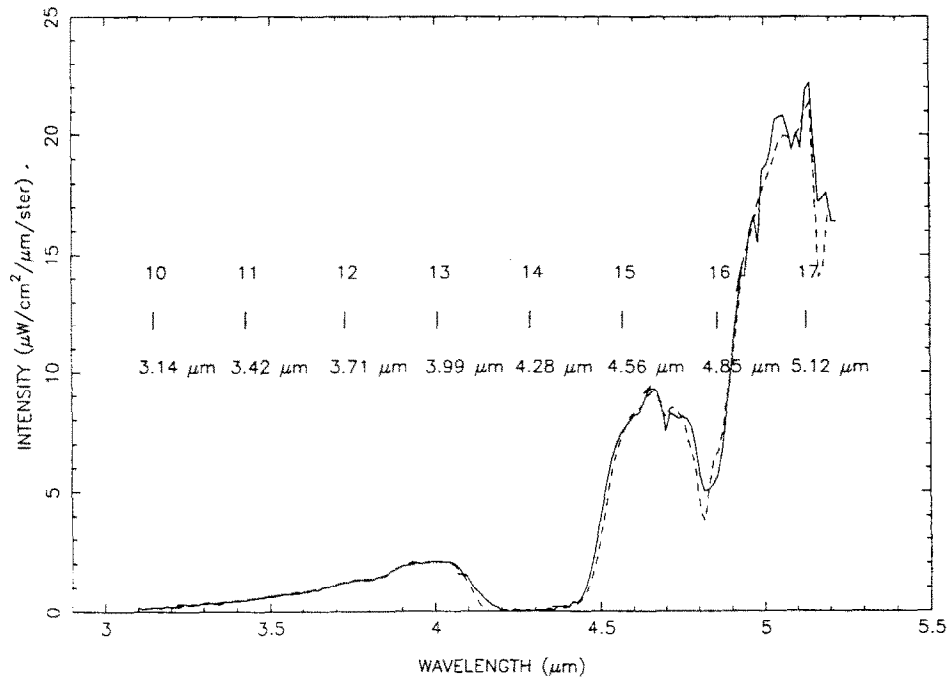


Fig. 1. Example of a VJBARS spectrum (solid line). The bars correspond to the positions of the VPDIN bands. The absorptions at 4.3 and 4.8 μm are due to the CO_2 ν_1 and $\nu_1 + \nu_2$ bands. A synthetic spectrum, calculated with the nominal thermal profile, is shown for comparison (dotted line)

bands at 4.3 μm ; an example of a typical curve is shown in Fig. 2 (circles), where the flux in each channel is plotted against the emission angle.

A model study of the limb-darkening effect has been performed by Diner (1978) and Taylor *et al.* (1980) for a semi-infinite plane-parallel atmosphere, between 8 and 20 μm . The model assumes no gaseous absorption, and is

thus relevant to the wavelengths at which the upper cloud continuum is reached, between the atmospheric absorption bands, in the 3–5 μm region (this excludes also the 4.845 μm CO_2 absorption band, which is analysed for thermal structure determination below).

The absorbing particles are assumed to have an exponential density distribution above a reference altitude z_0 ,

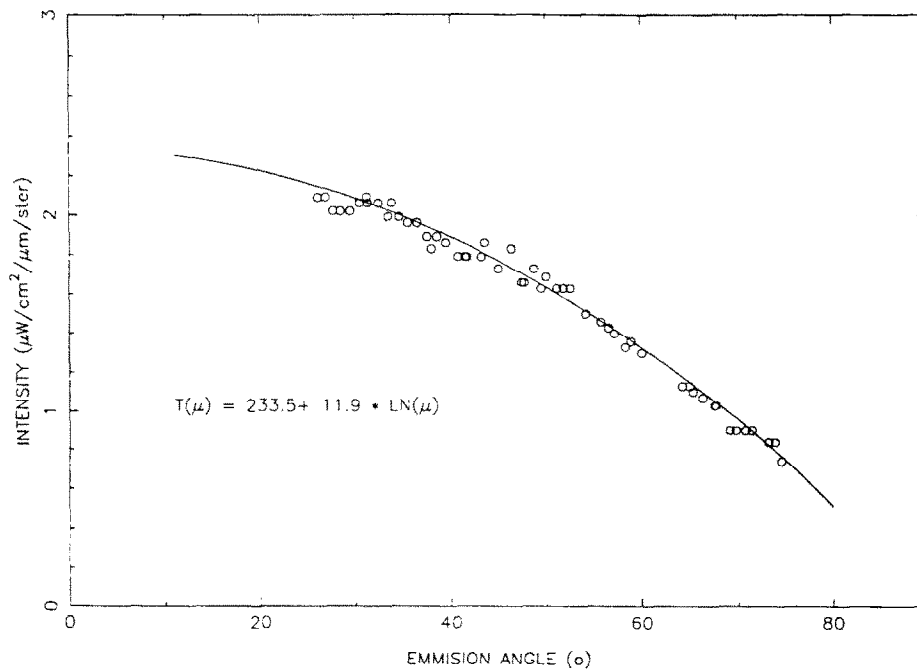


Fig. 2. Example of limb-darkening profile at a wavelength of 4.00 μm (Channel 13) and at a latitude of -0.3° . The circles correspond to the NIMS measurements, and the solid line to the best fit obtained with equation (3), with $T_1 = 233.5$ and $C = 11.9$ (see text)

with a particle scale height H , constant over the altitude range probed by the observations. The temperature lapse rate at a given latitude is also assumed to be constant over a cloud scale height, which is expected to be of the order of a few kilometres (Diner, 1978). Then, as shown by Diner (1978), the observed radiation mainly comes from a single effective level of altitude z , defined by a constant cloud optical depth, which depends upon the cosine of the emergence angle, μ , the cloud scale height H , and the altitude difference $z - z_0$:

$$\tau = \frac{\sigma N_0 H}{\mu} \exp\left(-\frac{z - z_0}{H}\right), \quad (1)$$

where σ is the aerosol cross-section and N_0 the particle density at level z_0 . Let $T(\mu)$ be the brightness temperature observed. It follows directly from equation (1) by expressing $z - z_0 = (T - T_0) \times dz/dT$, that:

$$T(\mu) = T_0 + \frac{dT}{dz} H \ln\left(\frac{H\sigma N_0}{\tau\mu}\right), \quad (2)$$

where T_0 is the temperature of reference for the level of altitude z_0 . The solution of the radiative transfer equation is such that, for each value of μ , the observed brightness temperature corresponds to $\tau = 1$. Therefore, $T(\mu)$ can be expressed as follows:

$$T(\mu) = T_1 + C \ln \mu, \quad (3)$$

where T_1 is the observed brightness temperature under normal incidence, having the following relation with T_0 : $T_1 = T_0 + dT/dz H \ln(H\sigma N_0)$, and $C = -H \times (dT/dz)$. Since the mean temperature gradient in Venus's atmosphere is negative (Seiff, 1983), the C factor is expected to be positive under nominal conditions. Figure 2 gives an example of the fit obtained for the expression of $T(\mu)$.

Observations of the limb-darkening, i.e. the curve $T(\mu)$, thus give access to the product $H \times (dT/dz)$. With this model, the two parameters T_1 and C are determined by fitting the limb-darkening curves in a least-square sense. More sophisticated four-parameter models have been used for the *Pioneer* Venus VORTEX experiment (Taylor *et al.*, 1980), but the more limited number of points in the case of the NIMS maps allows us to retrieve only the two most important parameters, T_1 and C . In this determination, it has been assumed that the gaseous opacity can be neglected. Where this is not the case, the complete determination of the limb darkening is achieved by using a band model, describing the Venus atmosphere, as for the synthetic spectra calculations described below. The band model used is a statistical band model with an inverse distribution of the intensities ("LS" model), which was developed for Martian atmosphere studies (Rosenqvist *et al.*, 1990). For the wavelength of 4.845 μm , which has been used here to check the thermal profile used (see below), it has been shown that the same logarithmic law for $T(\mu)$ is still valid, but the scale height now depends both on the cloud scale height and the atmospheric scale height.

It has also been assumed that the scattering effects within the clouds can be neglected (i.e. that the cloud particles are very absorbing). This assumption will be

discussed below, when comparison with complete models including scattering will be made.

In what follows, we will present a determination of the constant C for the various discrete thermal channels available in the VPDIN-1 mosaic, and at various latitudes. Then, using Seiff's nominal temperature profile, the cloud scale height will be extracted.

Analysis of the global mosaic data

The VPDIN-1 mosaic is used since it has the best latitude and emission angle coverage. The five continuum wavelengths which have been used for our analysis are given in Fig. 1. Channel 14 (4.279 μm) has not been used, because it lies in the CO_2 absorption bands. Channel 10 (3.140 μm) has also been ignored, because of a too low signal-to-noise ratio. As noted above, Channel 16 (4.845 μm), corresponding to a weaker CO_2 band, has nevertheless been included for the thermal structure determination.

For each wavelength and latitude, limb-darkening profiles have been fitted according to equation (3), by means of a least-square method, in order to retrieve T_1 , C and the associated error bars. It should be noted that, because of the spacecraft's orbital geometry, the observed emergence angle varies as a function of latitude. The subspacecraft latitude was +13.5°N at the time of the VPDIN-1 measurements. Thus, at this latitude, the minimum observed emergence angle is zero, μ is 1, and a direct measurement of T_1 can be made to compare with the least-square fit. Results are shown in Figs 3 and 4, for T_1 and C respectively.

To illustrate the method, Fig. 3b shows the Venus image at 4.00 μm , in cylindrical projection, juxtaposed with the T_1 latitudinal profile. The latitudinal contrasts correspond to variations in the cloud transmission or thermal structure, which correspond to variations in T_1 at these latitudes.

Figure 3a shows that the values of T_1 range from 230 to 240K, with a slight dependence on wavelength, for latitudes lower than 50°. The variation of T_1 with latitude is correlated for all values of λ . There is a slight asymmetry between the two hemispheres, T_1 being slightly higher in the Northern Hemisphere. It can be seen that T_1 tends to decrease toward high latitudes, poleward of $\approx 32^\circ\text{N}$ or $\approx 21^\circ\text{S}$, indicating that in these regions either the cloud level is higher, or the temperature at a given altitude is lower, or the cloud transmission is lower.

Figure 4 displays the value of the C factor as a function of latitude. The C curves are roughly symmetrical, and flat in a latitude range (25°S, 30°N). If extrapolated outside the probed latitude range, the C factor becomes close to zero at latitudes 40°S and 55°N. Since the scale height H is strictly positive, a null value of C can only be explained by a null value of the temperature lapse rate. Figure 4 thus suggests that at latitudes of 40°S and 55°N, the temperature lapse rate becomes quasi-isothermal above the upper cloud.

To retrieve the cloud scale height H from the value of C , a knowledge of the temperature lapse rate is needed.

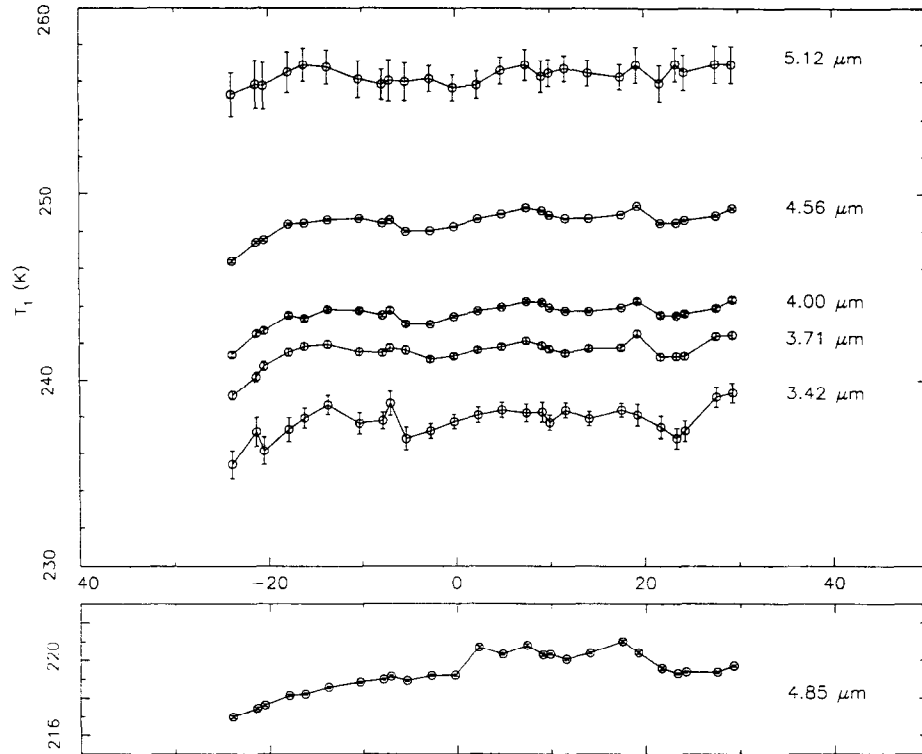


Fig. 3a. T_1 parameter as a function of latitude for the five wavelength channels. The wavelengths are indicated for each curve. Each curve is shifted from the next one by 5K. The ordinate scale corresponds to the lower curve. (b) (*Opposite*) The variations of T_1 as a function of latitude, for Channel 13 (3.99 μm), juxtaposed with the VPDIN-1 image in the same channel. Features in the image are places where the clouds are less prominent, thus giving rise to higher temperatures, and this is exactly what is seen in the T_1 curve

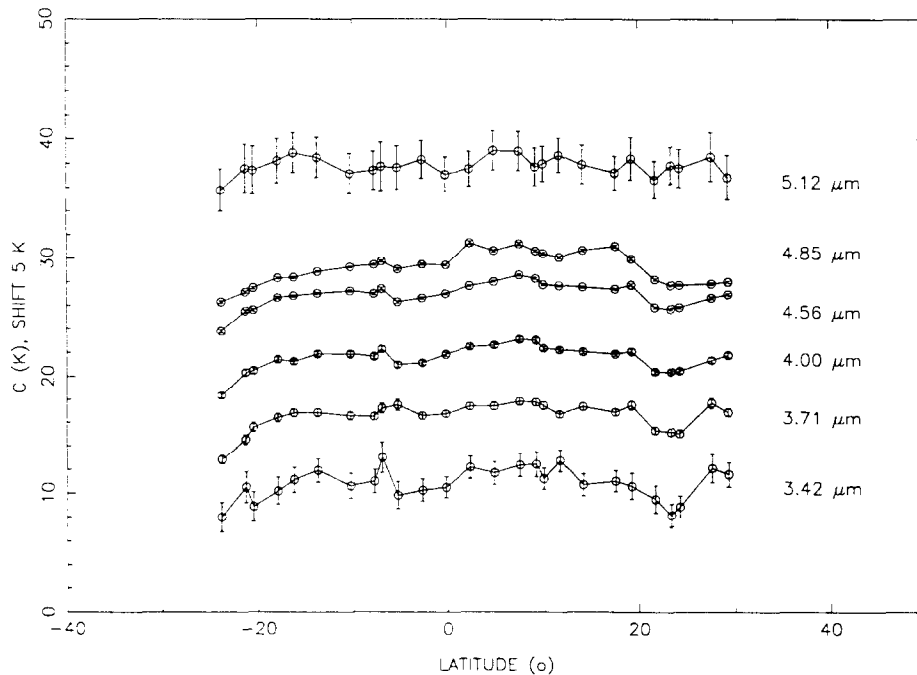


Fig. 4. Extraction of the C factor as a function of latitude for the five wavelength channels. Each curve is shifted from the next one by 5K. The ordinate scale corresponds to the lower curve

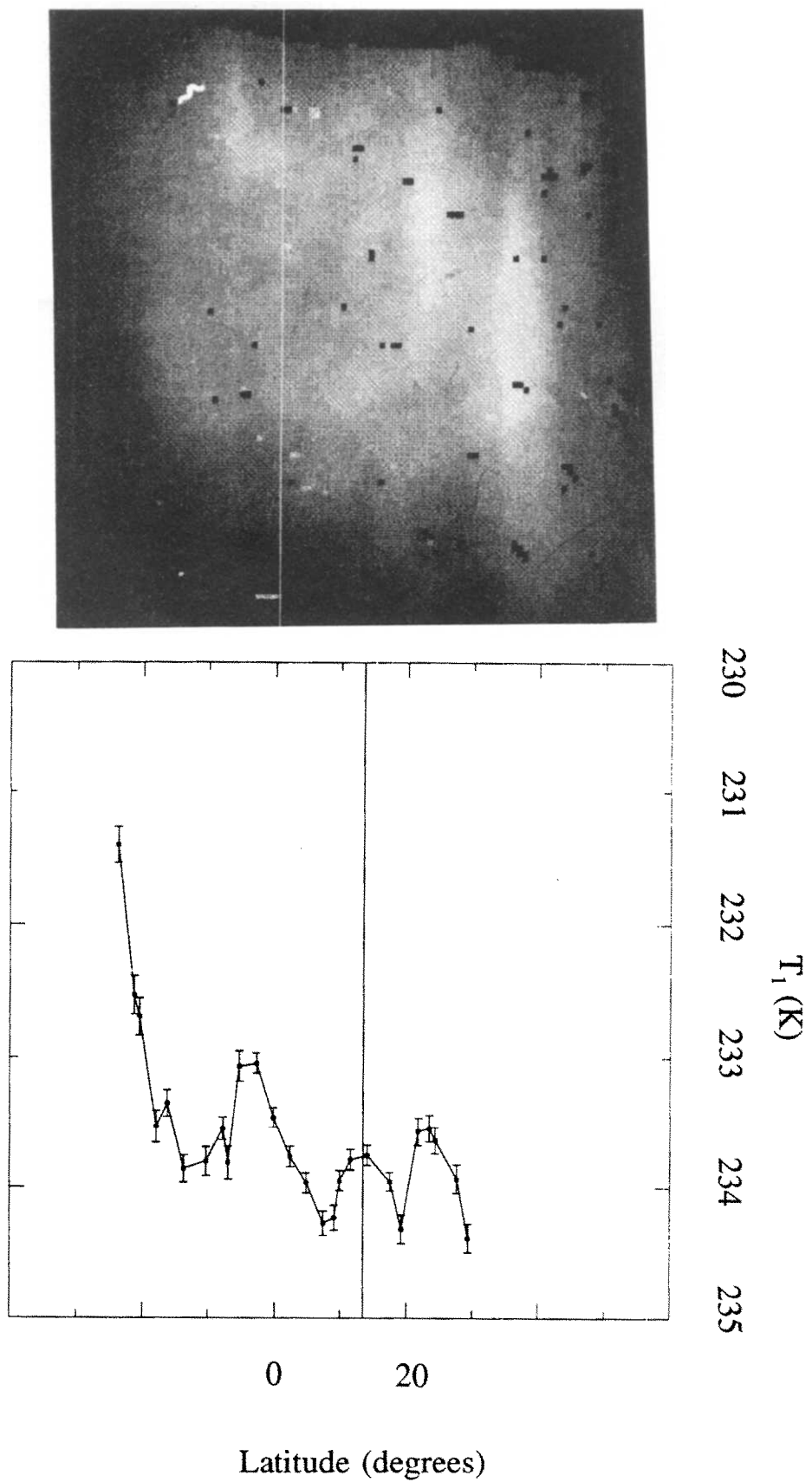


Fig. 3b.

In this paper, we have used the nominal thermal profile of Seiff (1983) in the latitude range studied (25°S , 30°N). The hypothesis of a constant thermal profile is checked by using the same limb-darkening method, but within the CO_2 band at $4.845\ \mu\text{m}$. In this case, it has been verified by means of synthetic spectra calculations, convolved to the NIMS instrumental response, that the same limb-darkening model does apply, but the constant $-C/(dT/dz)$ is no longer the cloud scale height. A complete band model synthetic limb-darkening profile has been calculated in this case, for an equatorial spectrum; the values of T_1 and C are: $T_1^{\text{calc}} = 217.8\text{K}$; $C^{\text{calc}} = 8.93\text{K}$, to be compared with the measured values: $T_1^{\text{meas}} = 219.3 \pm 1.5\text{K}$; $C^{\text{meas}} = 9.9 \pm 2.0\text{K}$ (error bars at 2σ). In these measurements, the error bars correspond to the observed latitudinal variations of the parameters. The conclusion of these measurements is therefore that both parameters are latitudinally constant within less than 2K . Since these constants now both depend on the thermal profiles at a higher altitude ($\approx 75\ \text{km}$), we conclude that the Seiff (1983) thermal profile is consistent with our measurements.

Analysis of the VJBARS spectra

A selection of 20 VJBARS spectra has been made over a latitude coverage ranging from 25°S to 35°N . An example of these spectra is shown in Fig. 1. The Venus spectrum between 3 and $5\ \mu\text{m}$ is characterized by two absorption bands of CO_2 , the strong, saturated ν_3 band centred at $4.3\ \mu\text{m}$, and the weaker $\nu_1 + \nu_2$ band centred at $4.8\ \mu\text{m}$.

Apart from these features, the spectrum approximately represents a blackbody, at a temperature close to the cloud temperature. However, the brightness temperature is not exactly constant over wavelength, as illustrated in Fig. 5; its variation reproduces, at first approximation, the variations of T_1 for the same latitude.

According to Seiff (1983), a brightness temperature of $230\text{--}240\text{K}$ corresponds to an altitude of $65\text{--}70\ \text{km}$. At the centre of the strong $4.3\ \mu\text{m}$ band, the radiation comes from an altitude of about $90\ \text{km}$, near the minimum temperature level which is close to 180K (Seiff, 1983). At the centre of the $4.8\ \mu\text{m}$ band, the probed level is about $75\ \text{km}$, i.e. a few km above the altitude of the upper cloud.

The continuum level at the wavelength of CO_2 band centre was estimated from a linear interpolation between two continuum levels at 4.659 and $4.968\ \mu\text{m}$ respectively. The average variations in the band depth as observed across the planet are about 6% . If the continuum level is constant, we can thus conclude that the temperature lapse rate does not vary by more than 6% in the (25°S , 30°N) latitude range. In the previous section it became clear that the variations of the cloud temperature are very small, and the constancy of the continuum level seems therefore a very reasonable hypothesis. Since the C factor is also found to be constant (within about 6%) in this region (Fig. 4), it can be inferred that the cloud scale height H is approximately constant in this latitude range.

To check the validity of the Seiff (1983) profile, synthetic calculations are performed at various latitudes. We have used a simplified radiative transfer scheme and band models, involving no scattering, previously used in the calculations presented by Carlson *et al.* (1991), which

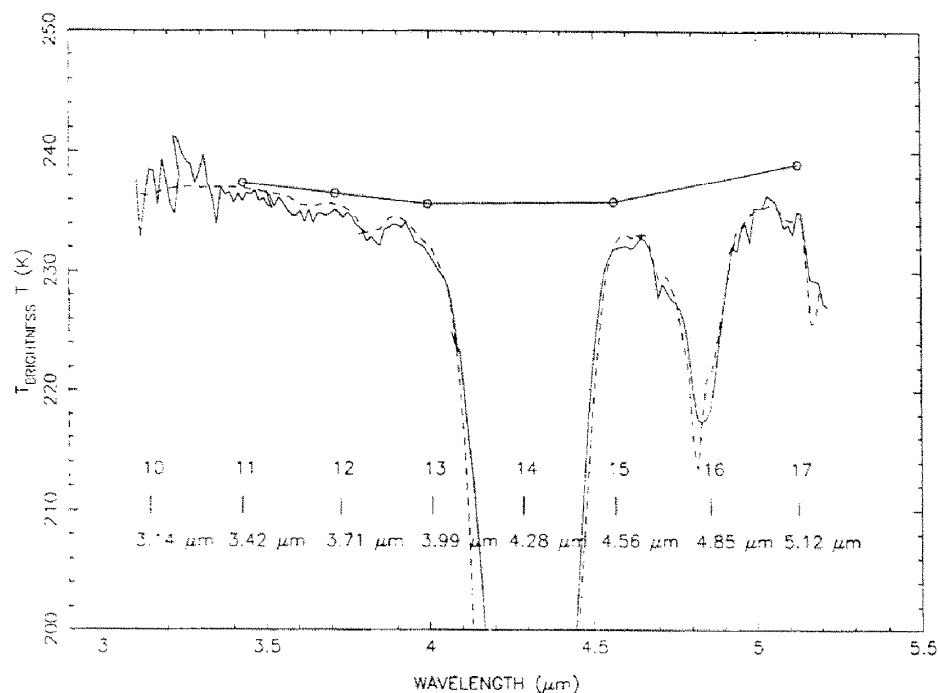


Fig. 5. Brightness temperatures as a function of wavelength for the VJBARS spectrum shown in Fig. 1. The latitude is $0.493\ \text{S}$. The superimposed solid line is the T^* value, which is derived from the T_1 value by corrections for gaseous absorption and the nonzero scale height effect in the radiative transfer equation. The T_1 values are taken from limb-darkening data at latitude $0.3\ \text{S}$. The dotted line is a synthetic spectrum, calculated using the nominal thermal profile

are expected to be adequate for calculating the outgoing intensity in the thermal channels. The CO₂ spectroscopic data are taken from the high-temperature database of Rothman (1986), Rothman *et al.* (1987) and Wattson and Rothman (1992).

The determination of the temperature lapse rate (averaged in the 60–80 km range), at the vertical resolution of the Seiff profile, has an uncertainty of 0.4 K km⁻¹ in the 60–80 km range, owing to the vertical resolution of the observations. Other input parameters are the upper cloud temperature (i.e. the temperature of the level corresponding to a cloud optical depth of unity) and the scale height of the upper cloud particles. As cloud temperature, we use the T_1 values derived at each latitude for our set of five wavelengths (excluding the CO₂ absorption at wavelength 4.845 μm), as illustrated in Fig. 3, and interpolated between these values. This allows us to calculate the synthetic spectrum corresponding to each latitude and to compare it with the observations. The influence of dT/dz is especially strong on the depth of the 4.8 μm CO₂ band, as mentioned above, and also on the red wing of the strong 4.3 μm CO₂ band.

The quality of the fit (Fig. 1) shows that the use of Seiff's nominal profile provides a satisfactory agreement with the data. On the other hand, no substantial variation in temperature nor lapse rate has been found from the limb-darkening fit at 4.85 μm, and we can safely use this thermal profile at all the latitudes included in this study.

Results and discussion

Determination of the cloud scale height

A simple method for deriving H consists of dividing, for each spectral channel and at each latitude, the C factor by the mean temperature gradient of Seiff's profile above the cloud ($dT/dz = -2.9 \pm 0.4$ K km⁻¹). We take the value of dT/dz , as given by Seiff's nominal model, with an average over the altitudes sounded at these wavelengths. The uncertainties come mainly from the vertical spacing of the data. As mentioned above, this result is remarkably constant in the range (25 S, 30 N). By taking its mean value over this latitude range, one obtains:

$$H = 4.1 \pm 0.6 \text{ km.}$$

Our determination of C ($C = 11.89$ K) is close to the value derived in our preliminary analysis ($C = 11.8$ K; Carlson *et al.*, 1991). However, a different temperature gradient was used in this reference ($dT/dz = -4.3$ K km⁻¹, implying a lower value of H). The present analysis uses a more accurate radiative transfer model, over a much larger sample of NIMS data, and is believed to be more reliable.

This determination of the scale height is made within the frame of the model of Diner (1978), which approximates the radiative transfer within the cloud by neglecting the scattering. This model is fully correct only for small enough single-scattering albedo of cloud particles. In the next section, we will derive a more accurate value of the

scale height by taking into account fully the scattering properties of cloud particles within a two-stream approximation. The approximate method described above has been used to derive the scale height at individual latitudes, because it gives a much faster computational time, whereas the complete scattering model has been used only on the latitudinal average. The relative variations of the scale height, within the latitude range (25°S, 30°N), are found to be less than 20%, a result which is not expected to change when scattering effects are taken into account. Therefore, we have limited ourselves to the calculation of the scattering within the full latitude range.

Estimate of the scale height including the scattering effects

The above analysis has shown that the particle scale height has an essentially constant value at low latitudes. Here, we apply a more accurate radiative transfer program to obtain an improved value for the particle scale height. The major reason for needing to use a more sophisticated radiative transfer code is that the cloud particles scatter as well as absorb and emit thermal radiation at the wavelengths of interest. For example, in the cloud model employed below, they have a single-scattering albedo of 0.5 at a wavelength of 3.7 μm, the central wavelength of NIMS Channel 12. As a result, the scale height inferred from the limb-darkening data is somewhat larger (by about 1 km) than that derived by neglecting particle scattering, as has been done up until now.

We used the two stream/source function solution to the radiative transfer problem for an inhomogeneous atmosphere to evaluate the specific intensity at the top of Venus's atmosphere as a function of μ , the cosine of the emission angle (Pollack *et al.*, 1993). Mie scattering theory was used to determine the single-scattering properties of the various size modes of the cloud particles. Almost all the radiation observed in the long-wavelength channels of the NIMS experiment originates from the region of the upper cloud and above. For reasons detailed in Grinspoon *et al.* (1993), we considered the upper cloud to be composed of a uniform mixture of mode 1 and mode 2 particles (modal radii equal to 0.3 and 1.0 μm, respectively), with the mode 1 and 2 particles contributing 15% and 85%, respectively, to the upper cloud opacity at a wavelength of 0.63 μm. For this choice of relative abundances, the mode 2 particles totally dominate the cloud opacity in the long-wavelength NIMS channels, as the extinction efficiency of the mode 1 particles decreases much more rapidly with increasing wavelength than does that of the mode 2 particles.

To obtain good statistics, we binned all the NIMS pixels in VPDIN-1 that lie between 0° and 30° N latitude into μ bins having a constant width of 0.05. We focussed on Channel 12 because the data in this channel has a good signal-to-noise ratio and because gas absorption is very small at the wavelength of 3.7 μm. [However, we did allow for gas absorption by using an appropriate set of correlated k distributions—see Grinspoon *et al.* (1993)]. The limb-darkening data derived in this way is shown in Fig. 6 by the solid curve through the centroids of the

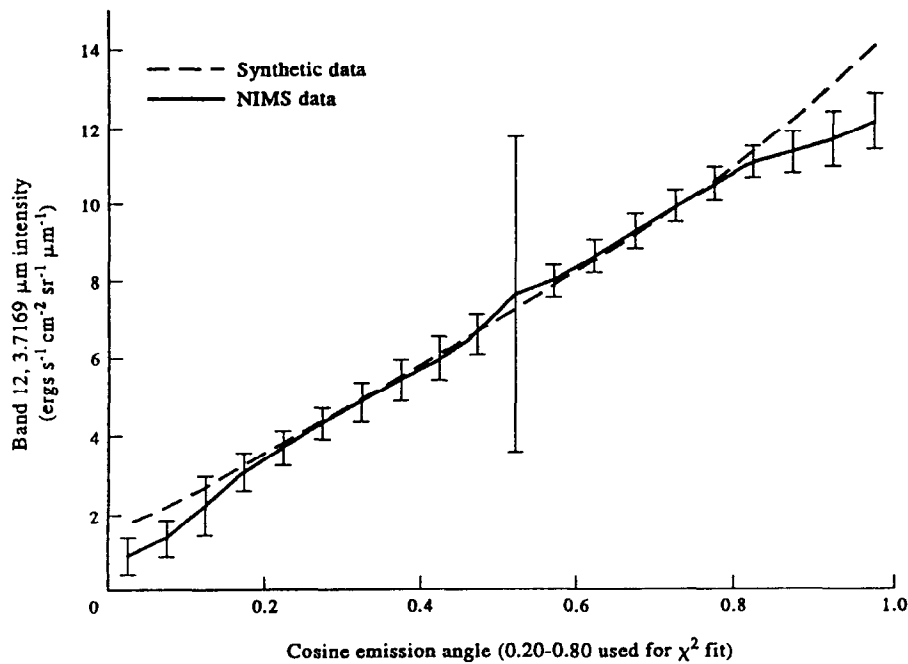


Fig. 6. Comparison of the limb darkening observed in NIMS Channel 12 ($3.717 \mu\text{m}$) for latitudes between 0° and 30°N (solid curve with error bars) with an optimized model (dotted curve) for the upper cloud consisting of a mixture of mode 1 and 2 particles (see text). The error bars represent the standard deviation of the intensity of the individual data points within a given cosine (emission angle) bin. The large central bar represents the spatial variations of the intensity within the selected area

individual binned data (vertical lines with error bars). The centroid of the lines is the mean value of the intensity for all the NIMS pixels that fall within a given μ bin and the distance between this centroid and the top (or bottom) of the error bar represents the variance in the intensity from this mean.

We obtained a best fit to these data between $\mu = 0.2$ and 0.8 by finding the values of two free cloud parameters that minimized the χ^2 value of the fit. These two parameters are the pressure at optical depth unity in the visible ($0.63 \mu\text{m}$), P_1 , and the particle scale height, H_p . The reasons for limiting the μ region of the fitting are discussed in Grinspoon *et al.* (1993) (also see below). Our best-fit model is shown by the dotted curve in Fig. 6. It is characterized by P_1 equal to 24 mbar (corresponding to a pressure of optical depth unity at $3.17 \mu\text{m}$ of 44 mbar), H_p equal to 5.26 km, and the normalized χ^2 equal to 0.046 (a value of 1 would be expected if all the variance was due to noise; this low value therefore indicates either an underestimation of noise, or, more probably, the presence of systematic errors in the model). The formal error bars on the above parameters are of the order of 0.1%, although in reality the true errors are much larger due to idealizations made in the cloud model. The increasing deviation of the optimized model from the data at $\mu > 0.8$ may be due to a change in the particle scale height at an altitude of about 63 km, with the scale height becoming much smaller than the derived value of H_p at lower altitudes. This matter is explored in Grinspoon *et al.* (1993). In this more complicated model, H_p increases by about 0.3 km. This increase may provide a more realistic estimate of the true uncertainty in H_p . Also, P_1 decreased by about 0.5 mbar.

On the other hand, the uncertainty in the cloud structure discussed above will also introduce an uncertainty in the scale height. An estimate of the total uncertainty in the scale height will be given by the error bar discussed in the model without scattering, which is about 15%. It includes both the small latitudinal variability, the thermal profiles' uncertainties and the variance in the data.

Comparison with Pioneer Venus data

In his analysis of ground-based infrared data, Diner (1978) found $H = 4.5 \text{ km}$, which therefore compares well with our measurement without scattering, which uses the same model. We therefore conclude that there is a good agreement between both data sets, and that the properties of the upper clouds of Venus have not varied between both observations.

A review of the *Pioneer Venus* (PV) results can be found in Esposito *et al.* (1983). *Pioneer* data show that the particles in the upper cloud layer have a bimodal size distribution—mode 1 particles having a modal radius of a few tenths of a micron and mode 2 particles having a modal radius of about $1 \mu\text{m}$ (Knollenberg and Hunten, 1979, 1980; Kawabata *et al.*, 1980). Mode 2 particles are the chief source of visible opacity, except at the highest altitudes [above about 80 km—Esposito *et al.* (1983); Venus International Reference Atmosphere, Seiff *et al.* (1986); Crisp (1986)]. Thus, the scale heights inferred from the NIMS limb-darkening law probably reflect chiefly the vertical distribution of mode 2 particles, a result that is in agreement with the scattering model described

in the previous section, and with the results of Grinspoon *et al.* (1993).

Variations of T_1 as a function of wavelength

To interpret T_1 as a cloud temperature, corrections for gaseous absorption and the effect of the scale height in the radiative transfer equation have to be made. The corrected temperature T_1^* is shown in Fig. 5, superimposed over a NIMS spectrum in the 3–5 μm range. Since T_1^* refers to the atmospheric level where the cloud optical depth is equal to unity, and is therefore free of gaseous contribution, we would expect the variations of T_1^* , which are of the order of 2.5K, to be correlated with the cloud opacity. The difference between T_1 and T_1^* is too small to have an observable effect on the determination of the scale height, through a variation of the temperature gradient between the atmospheric levels corresponding to T_1 and T_1^* . The general shape of T_1^* is shown in Fig. 5; it seems to imply that the opacity of the cloud is a maximum around 4 μm , where T_1^* is minimum, and that the opacity then decreases toward longer wavelengths. Previous study of Venus's reflectivity in the 2.5–4.0 μm range (Pollack *et al.*, 1978) found a good agreement with a composition of sulphuric acid with concentration of about 84%. We have presently no explanation for this behaviour. If confirmed by complete modelling using radiative transfer with scattering effects, this behaviour could imply the presence of another constituent mixed with the sulphuric acid.

Conclusion

In this paper, we have used both the NIMS global mosaic (VPDIN-1) and the full spectral resolution data (VJBARS) in order to derive the particle scale height of the cloud, and constraints on the thermal structure variations. From the limb-darkening curves in the 3–5 μm range, derived at various latitudes, an estimate of the product $(dT/dz) \times H$ is derived. A study of full-resolution spectra, taken at the same latitudes, shows that the thermal profile is approximately constant in the latitude range (25 S, 30 N), with a mean absolute gradient of -2.9K km^{-1} at altitudes of 65–75 km, consistent with the reference profile of Seiff (1983). The mean cloud scale height, averaged over latitude, is 5.2 km, within 15% accuracy.

At high latitudes, the limb-darkening method cannot be used for a determination of the cloud scale height, because dT/dz becomes close to zero, i.e. an isothermal profile above the upper cloud. The analysis of the upper thermal structure in the polar regions is being studied by other means and results will be presented in a forthcoming paper.

References

- Carlson, R. W., Baines, K. H., Encrenaz, Th., Taylor, F. W., Drossart, P., Kamp, L. W., Pollack, J. B., Lellouch, E., Collard, A. D., Calcutt, S. B., Grinspoon, D. H., Weissman, P. R., Smythe, W. D., Ocampo, A. C., Danielson, G. E., Fanale, F. P., Johnson, T. V., Kieffer, H. H., Matson, D. L., McCord, T. B. and Soderblom, L. A., *Galileo* infrared imaging spectroscopy measurements at Venus. *Science* **253**, 1541–1548, 1991.
- Carlson, R. W., Weissman, P. R., Smythe, W. D. and Mahoney, J. C., Near-infrared mapping spectrometer experiment on *Galileo*. *Space Sci. Rev.* **60**, 457–502, 1992.
- Crisp, D., Radiative forcing of the Venus mesosphere I. Solar fluxes and heating rates. *Icarus* **67**, 484–514, 1986.
- Diner, D. J., The equatorial and polar limbdarkening of Venus in the 8–20 μm region. *J. Atmos. Sci.* **35**, 2356–2361, 1978.
- Esposito, L. W., Knollenberg, R. G., Marov, M. Y., Toon, O. B. and Turco, R. P., The clouds and hazes of Venus, in *Venus* (edited by D. M. Hunten *et al.*), pp. 484–564. University of Arizona Press, Tucson, AZ, 1983.
- Grinspoon, D. H., Pollack, J. B., Sitton, B., Carlson, R. W., Kamp, L. W., Baines, H., Encrenaz, Th. and Taylor, F. W., Probing Venus's cloud structure with *Galileo*—NIMS. *Planet. Space Sci.* **41**, 515–542, 1993.
- Kamp, L., Taylor, F. W. and Calcutt, S., Structure of Venus' atmosphere from modelling of night-side infrared spectra. *Nature, Lond.* **336**, 360–362, 1988.
- Kawabata, K. D., Coffeen, D. L., Hansen, J. E., Lane, W. A., Sato, M. and Travis, L. D., Cloud and haze properties from *Pioneer* Venus polarimetry. *J. Geophys. Res.* **85**, 8129–8140, 1980.
- Knollenberg, R. G. and Hunten, D. M., Clouds of Venus: particle size distribution measurements. *Science* **203**, 792–795, 1979.
- Knollenberg, R. G. and Hunten, D. M., Microphysics of the clouds of Venus: results of the *Pioneer* Venus particle size spectrometer experiment. *J. Geophys. Res.* **85**, 8039–8058, 1980.
- Pollack, J. B., Strecker, D. W., Witterborn, F. C., Erickson, E. F. and Baldwin, B. J., Properties of the clouds of Venus as inferred from airborne observations of its near-infrared reflectivity spectrum. *Icarus* **34**, 28–45, 1978.
- Pollack, J. B., Dalton, J. B., Grinspoon, D. H., Wattson, R. B., Freedman, R., Crisp, D., Allen, D. A., Bézard, B., de Bergh, C., Giver, L. P., Ma, Q. and Tipping, R., Near infrared light from Venus' nightside: a spectroscopic analysis. *Icarus* **103**, 1–42, 1993.
- Rosenqvist, J., Bibring, J.-P., Combes, M., Drossart, P., Encrenaz, Th., Erard, S., Forni, O., Gondet, B., Langevin, Y., Lellouch, E., Masson, P. and Soufflot, A., The vertical distribution of carbon monoxide on Mars from the ISM-*Phobos* experiment. *Astron. Astrophys.* **231**, L29–L32, 1990.
- Rothman, L. S., Infrared energy levels and intensities of carbon dioxide. Part 3. *Appl. Opt.* **25**, 1795–1816, 1986.
- Rothman, L. S., Gamache, R. R., Goldman, A., Brown, L. R., Toth, R. A., Pickett, H. M., Poynter, R. L., Flaud, J.-M., Camy-Peyret, C., Barbe, A., Husson, N., Rinsland, C. P. and Smith, M. A. H., The Hitran data base: 1986 edition. *Appl. Opt.* **26**, 4058–4097, 1987.
- Seiff, A., Thermal structure of the atmosphere of Venus, in *Venus* (edited by D. M. Hunten *et al.*), pp. 215–279. University of Arizona Press, Tucson, AZ, 1983.
- Seiff, A., Schofield, J. T., Kliore, A. J., Taylor, F. W., Limaye, S. S., Revercomb, H. E., Sromovsky, L. A., Kerzhanovich, V. V., Moroz, V. I. and Marov, M. Ya., Models of the structure of the atmosphere of Venus from the surface to 100 kilometer altitude, in *Venus International Reference Atmosphere* (edited by A. D. Kliore, V. I. Moroz and G. M. Keating), pp. 3–58. Pergamon Press, Oxford, 1986.
- Taylor, F. W., Beer, R., Chahine, M. T., Diner, D. J., Elson, L. S., Haskins, R. D., McCleese, D. J., Markonchik, I. V., Reichley, P. E., Bradley, S. P., Delderfield, J., Schofield, J. T., Farmer, L. B., Froidevaux, L., Leung, J., Coffey, M. T. and Gille, J. C., Structure and meteorology of the middle atmosphere of Venus: infrared remote sensing from the *Pioneer* Orbiter. *J. Geophys. Res.* **85**, 7963–8006, 1980.
- Wattson, R. B. and Rothman, L. S., Direct Numerical Diagonalization: wave of the future. *J. Quant. Spectrosc. rad. Transfer* **48**, 763–780, 1992.